Research Article | Vol. 10, No. 10 / 1 October 2019 / Biomedical Optics Express 5325
Biomedical Optics EXPRESS

Automated accurate lumen segmentation using L-mode interpolation for three-dimensional intravascular optical coherence tomography

ARSALAN AKBAR,[1] T. S. KHWAJA,[2] AMMAR JAVAID,[1] JUN-SUN KIM,[3] AND JINYONG HA[1,2,*]

[1]Graduate School of Optical Engineering, Sejong University, 209 Neungdong-ro, Gwangjin-gu, Seoul 05007, South Korea
[2]Department of Electrical Engineering, Sejong University, 209 Neungdong-ro, Gwangjin-gu, Seoul 05007, South Korea
[3]Division of Cardiology, Severance Cardiovascular Hospital, Yonsei University College of Medicine, Yonseiro 50–1, Seodaemun-gu, Seoul 03722, South Korea
*jinyongha@sejong.ac.kr

Abstract: Intravascular optical coherence tomography (IVOCT) lumen-based computational flow dynamics (CFD) enables physiologic evaluations such as of the fractional flow reserve (FFR) and wall sheer stress. In this study, we developed an accurate, time-efficient method for extracting lumen contours of the coronary artery. The contours of cross-sectional images containing wide intimal discontinuities due to guide wire shadowing and large bifurcations were delineated by utilizing the natural longitudinal lumen continuity of the arteries. Our algorithm was applied to 5931 pre-intervention OCT images acquired from 40 patients. For a quantitative comparison, the images were also processed through manual segmentation (the reference standard) and automated ones utilizing cross-sectional and longitudinal continuities. The results showed that the proposed algorithm outperforms other schemes, exhibiting a strong correlation (R = 0.988) and overlapping and non-overlapping area ratios of 0.931 and 0.101, respectively. To examine the accuracy of the OCT-derived FFR calculated using the proposed scheme, a CFD simulation of a three-dimensional coronary geometry was performed. The strong correlation with a manual lumen-derived FFR (R = 0.978) further demonstrated the reliability and accuracy of our algorithm with potential applications in clinical settings.

1. Introduction

Cardiovascular diseases are the primary cause of death worldwide, with more than 17 million deaths reported every year, a figure that is anticipated to rise to 23 million by 2030 according to the American Heart Association [1]. The primary reason for cardiovascular diseases is the growth of atherosclerotic plaques on the coronary artery wall and angiographic reduction in the lumen area of the blood vessel [2], leading to arterial occlusion and sudden death [3]. The detection of percent luminal stenosis (decrease in lumen area) is a key indicator for disease prevention. In treatments through clinical application, information regarding the lumen area can be decisive during pre-interventional evaluation for stent selection and enactment location [4]. Therefore, a quantitative evaluation of the lumen area is critical for both diagnosis and prognosis of cardiovascular diseases.

Intravascular optical coherence tomography (IVOCT) is a catheter-based high-resolution imaging modality that generates two-dimensional cross-sectional images of coronary arteries. IVOCT boasts fine spatial resolution and contrasts progressively, making it the imaging modality of choice for the diagnosis of coronary artery diseases [4]. An illustrative application is the anatomic assessment of the optimal approach toward revascularization for patients with coronary

#374542 https://doi.org/10.1364/BOE.10.005325
Journal © 2019 Received 5 Aug 2019; revised 14 Sep 2019; accepted 14 Sep 2019; published 23 Sep 2019

Biomedical Optics EXPRESS

stenosis and evaluation of stent implantation. An OCT-derived computational flow dynamics (CFD) simulation can help make additional physiologic assessment of the fractional flow reserve (FFR), which is considered the gold standard for evaluating the functional significance of lesions with intermediate stenosis, and lumen contour extraction is the essential first step in constructing the three-dimensional (3D) coronary geometry required for CFD simulation [5]. The diagnostic accuracies of CFD and analytical fluid dynamics methods in deriving the FFR from OCT have been evaluated, with both methods exhibiting a strong linear correlation with pressure-wire measured FFR [6]. Alternatively, a simple fluid dynamics equation has been shown to accurately discern functional myocardial ischemia from OCT-derived FFR with less processing time, but at the cost of accuracy [7].

Delineating the lumen contour in a sequence of IVOCT images is laborious if processed manually. A manual or semiautomatic analysis of every IVOCT pullback containing 271 images per sequence is time-consuming for a trained analyst in a core laboratory. Moreover, the inter-observer inconsistency leads to an inconsistency between segmentation results of the same IVOCT pullback [8]. For a rapid, repeatable, and comprehensive diagnosis, an automated lumen segmentation of the acquired image sequence is desired [9].

To this end, numerous suboptimal algorithms have been reported for lumen contour extraction. Gurmeric et al. [10] used an active contour model-based structure and performed threshold processing on the angular intensity distributions of an OCT image. Sihan et al. [11] used multiple Canny filters to detect the edges of a lumen boundary and linked or excluded edges based on a heuristic scheme. Ughi et al. [12,13] distinguished the lumen border on each A-line and then smoothed the contour points using a spline algorithm. Tsantis et al. [14] based their segmentation scheme on a Markov random field model [15] that iteratively augments a cost function using pixel-level estimation. Roy et al. [16] used a random walk algorithm to detect contours with particular emphasis on seed refinement. Wang et al. [17,18] modeled image segmentation as an optimization problem and used dynamic programming to solve it. The above schemes utilize spatial continuity of the arterial walls in the transverse cross-sectional plane (C-mode).

A key flaw common among the aforementioned algorithms and most others [19–21]is the failure to automatically detect lumen contours in images with wide intimal discontinuities due to shadows from guide wires, motion artifacts, or bifurcations. Usually, images with side branches and bifurcations are discarded, limiting the scope of assessment of the mother vessel lumen. Excluding such images increases the risk of losing critical information, whereas manual detection makes the segmentation process inefficient.

A recent approach toward feature extraction exploits the natural spatial continuity in the longitudinal axes of blood vessels. As a first step, a longitudinal cutaway view (L-mode) is created by collating the corresponding points on an arbitrary line in the sequence of images of a single pullback. In the scheme proposed by Athanasiou et al. [22,23], the cross-sectional lines of a transverse image at different angles were merged in sequence to create a longitudinal image. Alternatively, the average of all the intensities of the depth points of the transverse image can be collated, as demonstrated by Han et al. [24]. In both the schemes, guide wire, residual blood, or motion artifact discontinuities are identified as a sudden decrease in pixel intensity across frames. To our knowledge, there is no scheme that can perform interpolation over wide luminal discontinuities by utilizing the spatial continuity in three dimensions.

A fully automated, time-efficient algorithm to extract lumen contours for OCT-derived FFR computation is reported in this paper. Our algorithm is applied to OCT pullback sequences, including frames that exhibit wide intimal discontinuities. The proposed algorithm utilizes the spatial continuity in both the transverse (C-mode) and longitudinal cutaway (L-mode) views of OCT pullback frames, thus obtaining additional information for an accurate interpolation of the wide discontinuities. The lumen contours extracted using the proposed scheme are collated to form a three-dimensional (3D) coronary geometry of the imaged artery. The geometry is

Biomedical Optics EXPRESS

inputted to a commercial CFD simulator to calculate the FFR and evaluate the accuracy of the 3D geometry derived from the proposed algorithm.

2. Methods

The proposed lumen detection algorithm consists of three main steps: pre-processing of the raw OCT frames, side-branch tracing to generate longitudinal cutaway images for bifurcation frames, and morphological approach for final lumen extraction, as shown in Fig. 1.

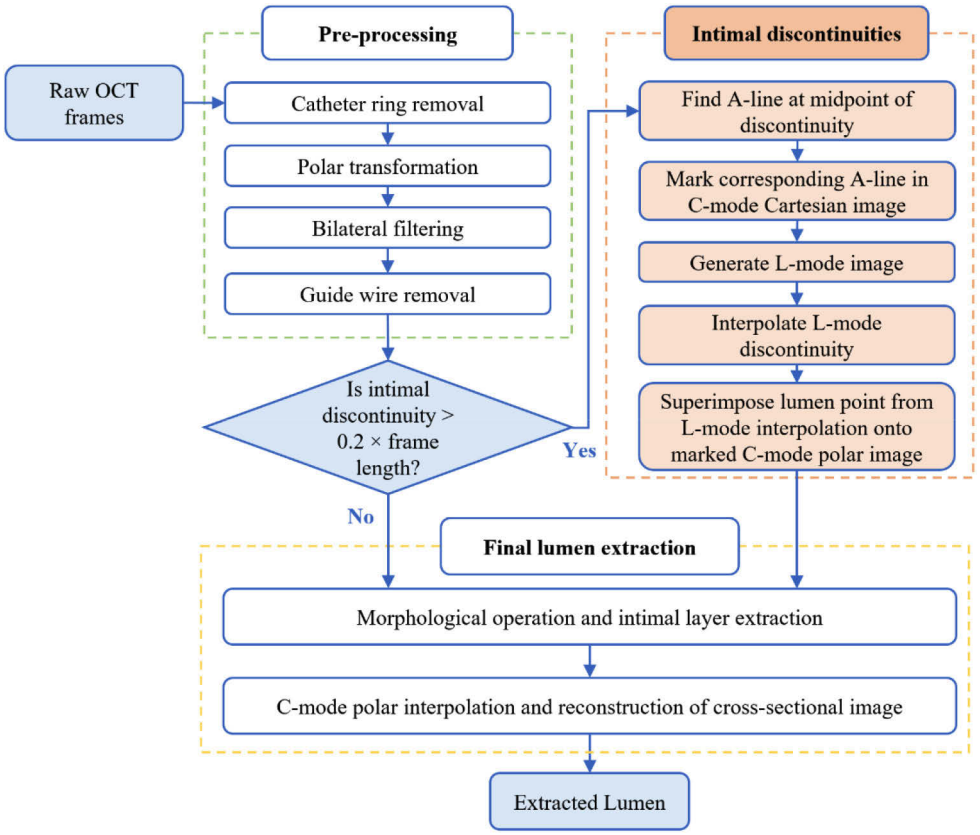

Fig. 1. Workflow of the proposed methodology.

2.1. Raw IVOCT dataset

The dataset to which our methodology was applied contained 40 pre-intervention IVOCT pullbacks (5931 frames) from 40 patients with intermediate stenosis in the left anterior descending artery (27 patients), in the right coronary artery (6 patients) and in the left circumflex artery (7 patients). The cross-sectional OCT images were acquired at a rate of 100 frames/s using a frequency-domain OCT system (C7-XR OCT imaging system, LightLab Imaging, Inc./Abbott Vascular, CA, USA). The fiber probe was pulled back at a speed of 20 mm/s within the transparent and stationary sheath. The size of each image was 1,024 × 1,024 pixels. Manual lumen, targeting main vessels subject to coronary disease for OCT-derived FFR, was extracted by two independent analysts with extensive experience in vascular segmentation.

Biomedical Optics EXPRESS

2.2. Pre-processing

Figure 2(a) shows an illustrative raw image. The pre-processing module performs catheter removal [25,26], polar transformation, and bilateral filtering [27], the result of which is shown in Fig. 2(b). Figure 2(c) shows the results of the initial binarization of the polar image [28].

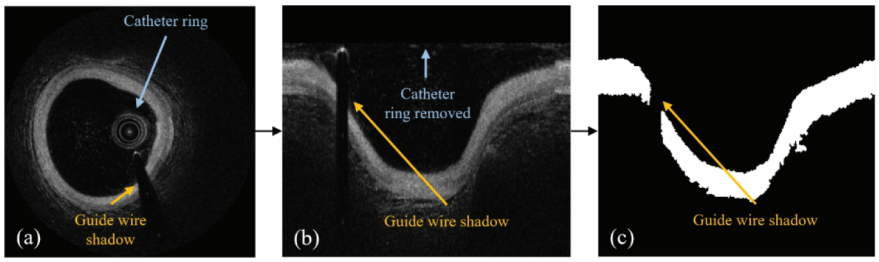

Fig. 2. (**a**) OCT C-mode frame in Cartesian coordinates with a catheter ring and guide wire shadow, (**b**) Polar-transformed C-mode image with the catheter ring removed, and (**c**) Binarized polar cross-section showing intimal discontinuity originating from the guide wire shadow.

2.3. Wide intimal discontinuities

C-mode interpolation over wide intimal discontinuities yields erroneous lumen extraction results. The discontinuities are primarily due to arterial bifurcations and the guide wire. A bifurcation alone, or when it overlaps the guide wire, can appear as a discontinuity wide enough to be unsuitable for processing via interpolation. Currently, to avoid under or over-segmentation, frames with wide discontinuities are manually identified and discarded. Here, we describe a method to process these frames by generating and utilizing the L-mode view of the OCT pullback.

To identify wide intimal discontinuities in a binarized polar-transformed image, each A-line of the frame should be scanned for lumen pixels. The number of successive A-lines without lumen is recorded. If the ratio of this recorded length to the total A-lines per frame exceeds 0.20, the frame is marked to be processed separately as a wide discontinuity.

A marked frame is processed as shown in Fig. 3. First, the bisecting A-line of the discontinuity is identified in the polar-transformed image (Fig. 3(a)). The corresponding A-line is used to determine the bisecting angle of the Cartesian image (Fig. 3(b)). At this angle, slices of ten preceding and ten succeeding frames are collated to generate an L-mode. To reduce the noise and for smoothing the L-mode image, bilateral filtering [27] is applied (Fig. 3(c)). The upper and lower clusters of the image are scanned for L-mode discontinuities. Once identified, a discontinuity is compensated using linear interpolation (Fig. 3(d)). The lumen point extracted by L-mode interpolation is superimposed onto the marked binarized polar frame (Fig. 3(e)). Therefore, through L-mode interpolation, the natural longitudinal continuity of the arterial wall is exploited to reduce the length of a cross-sectional intimal discontinuity by half.

Some L-mode cutaways contain narrow discontinuities because of longitudinal arterial bifurcations, leading to over-segmentation. The sample image in Fig. 4(a) shows endpoints of discontinuity displaced in the vertical axes. This leads to interpolant overshoot, derived-point overshoot, and over-segmentation, as shown in Fig. 4(b), Fig. 4(c), and Fig. 4(d), respectively. To delineate over such artifacts, an interpolation is carried out five pixels away from the endpoints, as shown in Fig. 4(e), thereby improving the derived lumen point in the C-mode, as shown in Fig. 4(f), and realizing a more accurate segmentation as shown in Fig. 4(g).

Biomedical Optics EXPRESS

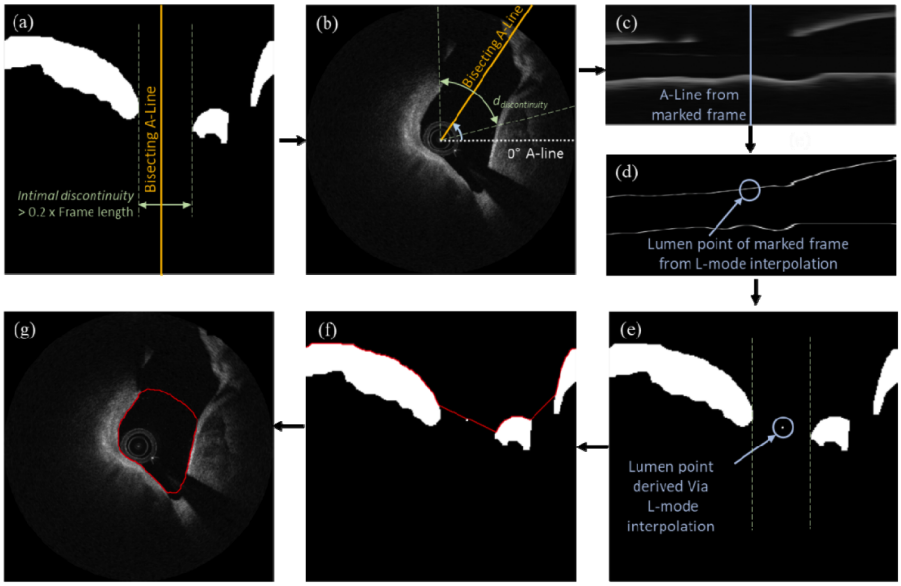

Fig. 3. (**a**) Frame marked as having a wide intimal discontinuity, (**b**) Angle of the A-line bisecting the discontinuity is identified, (**c**) L-mode image is generated by collating the corresponding A-lines of a sequence of frames, (**d**) L-mode interpolation, (**e**) Lumen point derived via L-mode interpolation is superimposed on a marked C-mode polar image, (**f**) C-mode interpolation, and (**g**) Extracted lumen contour.

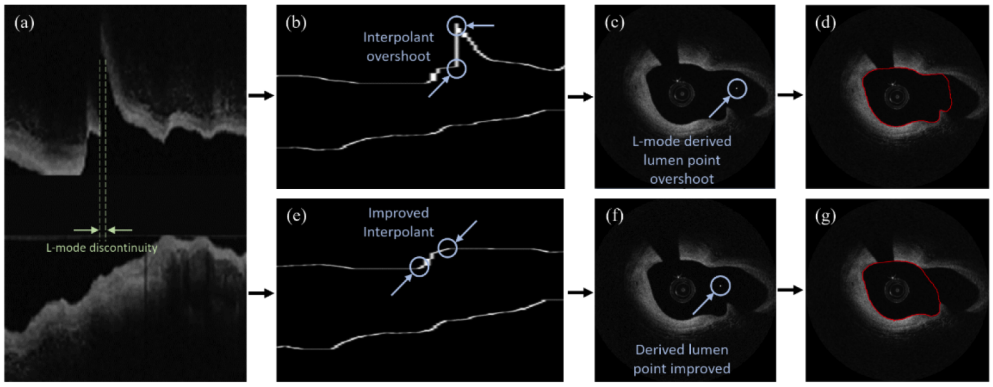

Fig. 4. (**a**) L-mode view showing narrow discontinuity, (**b**) Interpolation between endpoints leading to interpolant overshoot, (**c**) Derived point overshoot results in (**d**) overshoot of lumen contour; (**e**) Interpolation between points spaced five pixels away from the endpoint, resulting in improved interpolant, (**f**) Improved derived lumen point from L-mode interpolant, and (**g**) Improved lumen contour.

Biomedical Optics EXPRESS

2.4. C-mode interpolation and lumen extraction

The binarized polar frames, including those processed for wide intimal discontinuities, are subjected to a morphological dilation-erosion smoothing operation [25]. To initialize intimal layer extraction, top-most edge detection is conducted on each binarized A-line. This yield lumen extracted without accounting for the discontinuities. To remove the discontinuities, polar interpolation is applied to the frame. The lumen border points are then identified using the Sobel edge detection method [28], and the resulting polar image is transformed into a Cartesian image.

2.5. 3D reconstruction and OCT-derived FFR simulation

To construct the 3D coronary geometry, an in-house semiautomated software running on a Unity Real-Time Development Platform (Unity Technologies, SF, USA) was utilized. Figure 5(a) shows the coronary angiography of the left anterior descending artery imaged using OCT. The minimum lumen area (MLA) is indicated. Figure 5(b) shows the OCT frames derived from the proposed algorithm loaded into the software and placed at 0.2 mm intervals along their centerline. Equidistant points on each of the N contours are extracted, and a ray casting approach is applied to construct the mesh surfaces of the 3D lumen shown in Fig. 5(c).

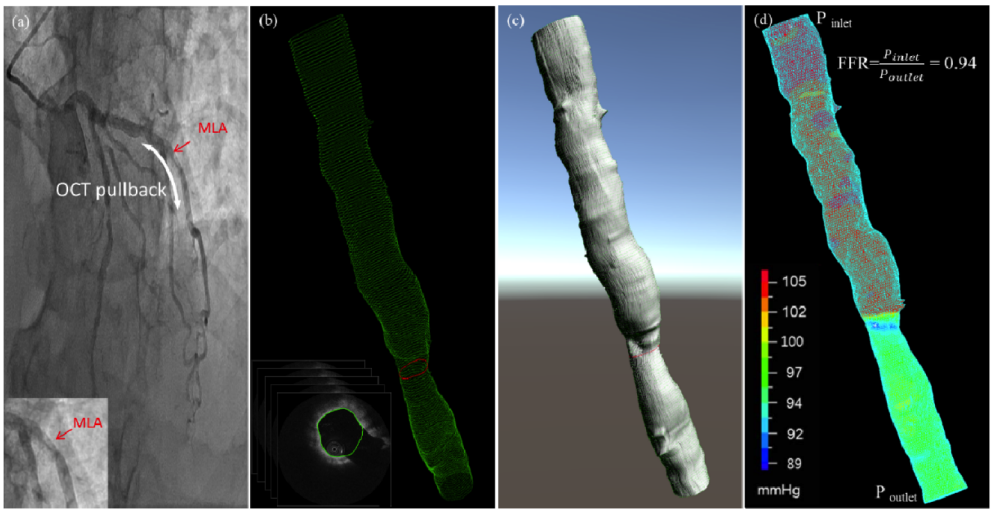

Fig. 5. CFD model and FFR simulation: (**a**) Coronary angiography of the left circumflex artery (**b**) Stacking of the OCT-derived lumens extracted using the proposed scheme, (**c**) 3D geometry after mesh generation, and (**d**) CFD computation for FFR calculation.

For a steady-state CFD analysis, the 3D geometry was inputted to a finite element analysis software (ADINA; ADINA R&D, Inc., Watertown, MA); the model has anisotropic meshes with tetrahedral elements. The blood flow simulation was processed to determine the arterial wall–blood flow interaction by applying the Navier–Stokes equations and a no-slip boundary condition. The velocities on the coronary angiograph were assessed using the thrombolysis in myocardial infarction frame count, and the mean flow velocity was calculated. To determine the mean blood pressure, the pressure acquired at the catheter tip in 37 lesions was averaged [5]. FFR_{OCT} was calculated as the ratio of the mean distal pressure to the mean proximal pressure. The calculated FFR_{OCT} was subsequently compared with manual lumen-derived FFR. Figure 5(d) shows the CFD simulation results of the coronary geometry, including a pressure map, and the FFR.

Biomedical Optics EXPRESS

3. Results

We proposed a novel lumen segmentation methodology in which the L-mode interpolants of frames containing wide intimal discontinuities were derived to halve the discontinuity prior to cross-sectional interpolation.

To evaluate the performance, the proposed scheme was compared with alternative methodologies reported in literature in terms of how efficiently they delineate the ground-truth manually segmented lumens. The existing methodologies were categorized into those that utilize cross-sectional image (C-mode) interpolation only [28] and those that utilize longitudinal cutaway (L-mode) interpolation only [23]. In another alternative scheme, the pullback frames were divided into several subsets, and the L-mode or C-mode interpolants were chosen based on the position correction procedure reported in [29].

Our scheme can be qualitatively assessed from exemplar segmentations with wide intimal discontinuities, as shown in Fig. 6. The figure shows the automatically extracted contours from all the three schemes juxtaposed with the manually delineated lumen. The segmentations based on the proposed methodology follow the manual contour closely, whereas those based on the C-mode or L-mode only schemes deviate from the reference contour within the discontinuity.

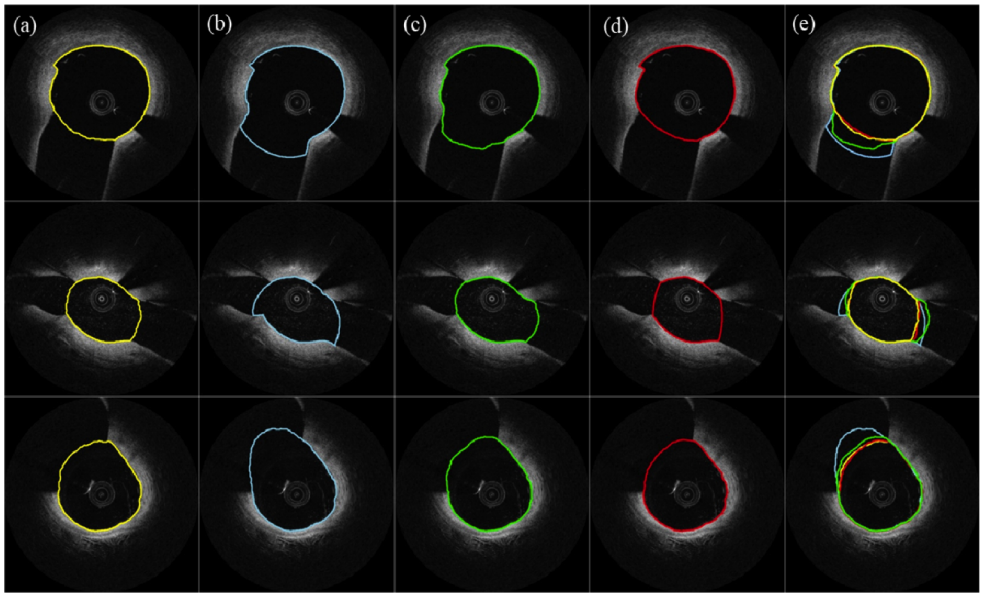

Fig. 6. Exemplar segmentations showing (**a**) Reference manual contour, (**b**) C-mode only contour, (**c**) L-mode only contour, (**d**) Contour delineated using the proposed methodology, and (**e**) Contours from schemes superimposed for comparison.

To evaluate the quantitative accuracy of the proposed algorithm, we set the ground truth reference contours as those derived from manual segmentation. Figure 7(a) shows the Pearson's correlation coefficient, R, of the proposed scheme interpolants and the C-mode interpolants with the manual contours. To highlight the novelty of the proposed scheme, the correlations with only wide intimal discontinuities are considered in Fig. 7(b).

Another metric was used to assess the accuracy of our scheme. This involved calculating the overlap (sensitivity) and non-overlap (specificity) ratios between the proposed and the manual segmentations. The overlap and non-overlapping ratios can be defined as follows.

$$R_{over} = \frac{TP}{TP + FN}, R_{non-over} = \frac{FN + FP}{TP + FN} \tag{1}$$

Biomedical Optics EXPRESS

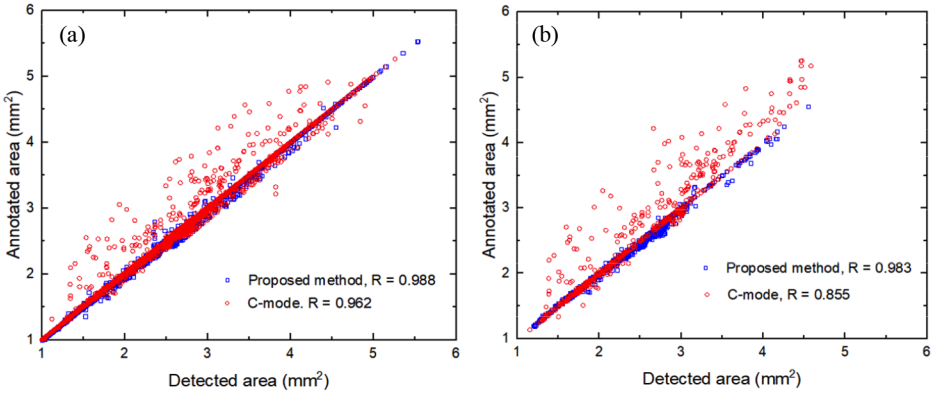

Fig. 7. Correlation graphs with manual segmentation as the gold standard, illustrating the segmentation accuracy with the proposed methodology versus that with C-mode only interpolants for (**a**) All frames of IVOCT pullback and (**b**) Frames containing wide intimal discontinuities.

Here, the common area included by the automatic and manual segmentation is taken as a true positive (TP), the area included by automatic but excluded by manual segmentation is taken as a false positive (FP), and the area excluded by automatic but included by manual segmentation is taken as a false negative (FN).

Table 1 lists a summary of the correlation, overlap ratio, and non-overlap ratio for each scheme. The proposed scheme provides the strongest correlation (0.988), maximum overlapping regions (0.931), and minimum non-overlapping regions (0.101) among the schemes. In particular, when the dataset is limited to wide discontinuities, the difference in the correlations is even more pronounced. Table 1 also lists the parameters evaluated for frames containing wide intimal discontinuities. Again, the proposed scheme gives the strongest correlation (0.983), maximum overlapping regions (0.931), and minimum non-overlapping regions (0.101).

Table 1. Comparison of Lumen Contours Extracted using the Proposed Scheme with those Extracted using C-mode Interpolation only, L-mode Interpolation only, and Position Correction. For Comparison, the Evaluation Parameters *R*, R_{over}, $R_{non-over}$, and Runtime (in s) are included. The Values inside the Brackets are those Obtained Considering Wide Discontinuity.

Methods	R	R_{over}	$R_{non-over}$	Runtime
C-mode interp. [28]	0.962	0.914	0.132	85
	(0.855)	(0.850)	(0.313)	
L-mode interp. [23]	0.971	0.902	0.113	228
	(0.952)	(0.920)	(0.230)	
Position correction [29]	0.982	0.921	0.108	315
	(0.978)	(0.915)	(0.187)	
Proposed scheme	0.988	0.931	0.101	176
	(0.983)	(0.931)	(0.101)	

Table 1 also lists the processing times of each algorithm. The proposed scheme executes the operation in 176 s, whereas the C-mode interpolation only takes 85 s by using core i5 desktop computer with 16 GB RAM.

The FFR was calculated by conducting a 3D CFD simulation. For the simulation, a 3D coronary geometry was derived using the proposed scheme. To examine the accuracy of the FFR calculated using the proposed scheme, its correlation with a manual lumen-derived FFR was

Biomedical Optics EXPRESS

determined. For comparison, the correlation of the C-mode FFR was also found. The strong correlation (R = 0.978) of the proposed scheme FFR indicates that it is in good agreement with the manual lumen-derived FFR (Fig. 8(a)). The C-mode FFR (R = 0.853) exhibits a weaker correlation, because of the inability to interpolate wide discontinuities. Figure 8(b) shows the illustrative example of CFD simulation results of the manual lumen-derived FFR, proposed scheme FFR, and C-mode FFR.

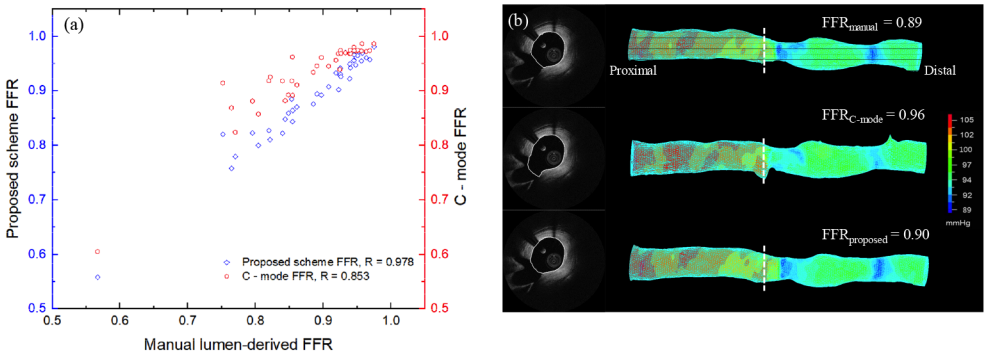

Fig. 8. (**a**) Correlation graphs with manual lumen-derived FFR as the gold standard, indicating the accuracy of the proposed scheme FFR over the C-mode FFR; (**b**) Illustrative example of CFD simulation of manual lumen-derived FFR, C-mode FFR, and proposed scheme FFR. Similar features of blood pressure can be seen in the manual lumen-derived CFD and proposed scheme CFD simulations; these are missing in the C-mode CFD simulation (circled).

4. Discussion

The proposed fully automatic lumen segmentation scheme was employed for OCT-derived FFR computation. The correlation and OCT-derived FFR of lumen extracted using the proposed and alternate schemes were compared. Numerous algorithms for lumen segmentation and 3D reconstruction have been reported [10–21] that fail to accurately delineate lumen contours with wide intimal discontinuities. By utilizing the proposed scheme, reliable 3D models can be constructed for OCT-derived FFR computation.

The discontinuity length to frame length ratio that was used to differentiate between narrow and wide intimal discontinuities was optimized to 0.20. The L-mode interpolation for wide discontinuities produces stronger correlation than the C-mode interpolation at the cost of processing penalty. The optimal discontinuity length to frame length ratio is found as the ratio where marginal gain in correlation accrued by longitudinal interpolation is maximized relative to cross-sectional interpolation. Quantitative analyses demonstrated that the correlation gain of the proposed scheme is maximized if a ratio of 0.20 is selected.

An added optimization challenge was selecting the number of frames to utilize for longitudinal interpolation. There were two key factors to consider. First, the effect of the number of frames on the correlation of extracted lumen was evaluated. Moreover, processing time penalty imposed using additional frames was considered. After the quantitative assessment of both these factors, the optimal number of frames to use for longitudinal interpolation was determined to be ten.

A key utility of the proposed scheme is that during the segmentation process, no frame is discarded. Figure 7(a) shows that the C-mode contour correlation (red circles) scatter is spread to the left of the optimal correlation of 1.0 and the C-mode interpolant overshoots in frames with wide discontinuities (Fig. 7(b)). Such frames were discarded in previous studies [12,13,29]; however, in this study, no frames are discarded. Further, the correlations (indicated by blue

Biomedical Optics EXPRESS

squares) generated using the proposed scheme closely follow the optimal correlation. This is validation that the proposed segmentation scheme is fully automated.

The proposed scheme is also demonstrated to be time efficient. Although C-mode interpolation is the fastest scheme (85 s), it does not utilize longitudinal continuity resulting in weak correlation, sensitivity, and specificity metrics. L-mode interpolation (228 s) and position correction (315 s) both utilize longitudinal continuity; however, longitudinal interpolated result is utilized after the CPU suffers time penalty. In our scheme, longitudinal interpolation is invoked solely when the discontinuity threshold is crossed, thereby making our system more time efficient (176 s), which is critical in clinical settings. The execution time can be reduced further by employing graphical processing units [23].

In a clinical setting for the treatment of borderline patients, FFR computation can be decisive for pre-interventional evaluation of stent enactment [4]. The scope of a standard OCT-derived FFR computation is limited to the main vessel that is subjected to coronary disease, i.e., at a side branch discontinuity the lumen contour should be interpolated to follow the main vessel cross-sections.

Both qualitative and quantitative assessments indicate that the proposed algorithm exhibits strong correlation with manual lumens and accurately computes OCT-derived FFR. In particular, Fig. 8(a) shows strong correlation between the manual lumen-derived FFR and the proposed scheme FFR ($R = 0.978$). Stronger FFR correlation can be ascribed to accurate interpolation of main vessels, particularly in frames with wide bifurcations ($R = 0.983$ in Fig. 7(b)). Correct 2D segmentation translates into accurate 3D reconstruction, precise OCT-derived FFR computation, and informed pre-interventional decision making in clinical settings.

The proposed segmentation scheme is adaptable and can incorporate other advanced segmentation modules. For example, images that contain stent implants can be interpolated by upgrading them to the *Final lumen extraction* module of the proposed scheme that incorporates stent detection tools similar to those proposed in [30]. An extension of this work can test the adaptability of the proposed scheme toward post intervention evaluation of stent implantation.

5. Conclusion

We presented a fully automatic, time-efficient lumen contour extraction technique that enables accurate lumen extraction from intracoronary OCT images containing wide intimal discontinuities (due to guide wire shadowing and large bifurcations), thus providing a precise 3D coronary artery geometry for CFD simulations. In our scheme, the L-mode interpolant is used to derive additional information before C-mode interpolation to halve the gap in wide intimal discontinuities. Compared with other methodologies, the proposed scheme for lumen extraction exhibited a strong correlation, near unity overlapping ratio, low non-overlapping ratio, and efficient processing time. A CFD simulation of a 3D coronary geometry generated using the proposed scheme was performed to determine the FFR. The determined FFR exhibited a strong correlation with a manual lumen-derived FFR. This shows the promising performance of our segmentation methodology with potential applications in clinical settings.

Funding

National Research Foundation of Korea (NRF-2017M3A9E9073370).

Disclosures

The authors declare that there are no conflicts of interest related to this article.

References

1. E. J. Benjamin, P. Muntner, A. Alonso, M. S. Bittencourt, C. W. Callaway, A. P. Carson, A. M. Chamberlain, A. R. Chang, S. Cheng, S. R. Das, F. N. Delling, L. Djousse, M. S. V. Elkind, J. F. Ferguson, M. Fornage, L. C. Jordan, S.

Biomedical Optics EXPRESS

S. Khan, B. M. Kissela, K. L. Knutson, T. W. Kwan, D. T. Lackland, T. T. Lewis, J. H. Lichtman, C. T. Longenecker, M. S. Loop, P. L. Lutsey, S. S. Martin, K. Matsushita, A. E. Moran, M. E. Mussolino, M. O'Flaherty, A. Pandey, A. M. Perak, W. D. Rosamond, G. A. Roth, U. K. A. Sampson, G. M. Satou, E. B. Schroeder, S. H. Shah, N. L. Spartano, A. Stokes, D. L. Tirschwell, C. W. Tsao, M. P. Turakhia, L. B. VanWagner, J. T. Wilkins, S. S. Wong, and S. S. Virani, "Heart disease and stroke statistics—2019 update: A report from the American Heart Association," Circulation **139**(10), e56–e528 (2019).

2. R. Virmani, A. P. Burke, A. Farb, and F. D. Kolodgie, "Pathology of the vulnerable plaque," J. Am. Coll. Cardiol. **47**(8), C13–C18 (2006).
3. J. Narula, M. Nakano, R. Virmani, F. D. Kolodgie, R. Petersen, R. Newcomb, S. Malik, V. Fuster, and A. V. Finn, "Histopathologic characteristics of atherosclerotic coronary disease and implications of the findings for the invasive and noninvasive detection of vulnerable plaques," J. Am. Coll. Cardiol. **61**(10), 1041–1051 (2013).
4. A. Karanasos, J. Ligthart, K. Witberg, G. van Soest, N. Bruining, and E. Regar, "Optical coherence tomography: Potential clinical applications," Curr. Cardiovasc. Imaging Rep. **5**(4), 206–220 (2012).
5. J. Ha, J. S. Kim, J. Lim, G. Kim, S. Lee, J. S. Lee, D. H. Shin, B. K. Kim, Y. G. Ko, D. Choi, Y. Jang, and M. Hong, "Assessing computational fractional flow reserve from optical coherence tomography in patients with intermediate coronary stenosis in the left anterior descending artery," Circ.: Cardiovasc. Interventions **9**(8), e003613 (2016).
6. S.-J. Jang, J.-M. Ahn, B. Kim, J.-M. Gu, H. J. Sung, S.-J. Park, and W.-Y. Oh, "Comparison of accuracy of one-use methods for calculating fractional flow reserve by intravascular optical coherence tomography to that determined by the pressure-wire method," Am. J. Cardiol. **120**(11), 1920–1925 (2017).
7. F. Seike, T. Uetani, K. Nishimura, H. Kawakami, H. Higashi, J. Aono, T. Nagai, K. Inoue, J. Suzuki, H. Kawakami, T. Okura, K. Yasuda, J. Higaki, and S. Ikeda, "Intracoronary optical coherence tomography-derived virtual fractional flow reserve for the assessment of coronary artery disease," Am. J. Cardiol. **120**(10), 1772–1779 (2017).
8. S. Fedele, G. Biondi-Zoccai, P. Kwiatkowski, L. Di Vito, M. Occhipinti, A. Cremonesi, M. Albertucci, L. Materia, G. Paoletti, and F. Prati, "Reproducibility of coronary optical coherence tomography for lumen and length measurements in humans (The CLI-VAR [Centro per la Lotta contro l'Infarto-VARiability] study)," Am. J. Cardiol. **110**(8), 1106–1112 (2012).
9. Z. Ping, Z. Tongjing, and L. Zhiyong, *Segmentation and Classification Method in IVOCT Images* (Atlantis Press, 2015).
10. S. Gurmeric, G. G. Isguder, S. Carlier, and G. Unal, "A New 3-D Automated Computational Method to Evaluate In-Stent Neointimal Hyperplasia in In-Vivo Intravascular Optical Coherence Tomography Pullbacks," in *Medical Image Computing and Computer-Assisted Intervention – MICCAI* 2009, G.-Z. Yang, D. Hawkes, D. Rueckert, A. Noble, and C. Taylor, eds., Lecture Notes in Computer Science (Springer Berlin Heidelberg, 2009), pp. 776–785.
11. K. Sihan, C. Botha, F. Post, S. de Winter, N. Gonzalo, E. Regar, P. J. W. C. Serruys, R. Hamers, and N. Bruining, "Fully automatic three-dimensional quantitative analysis of intracoronary optical coherence tomography," Cathet. Cardiovasc. Intervent. **74**(7), 1058–1065 (2009).
12. G. J. Ughi, T. Adriaenssens, K. Onsea, P. Kayaert, C. Dubois, P. Sinnaeve, M. Coosemans, W. Desmet, and J. D'hooge, "Automatic segmentation of in-vivo intra-coronary optical coherence tomography images to assess stent strut apposition and coverage," Int. J. Cardiovasc Imaging **28**(2), 229–241 (2012).
13. G. J. Ughi, T. Adriaenssens, W. Desmet, and J. D'hooge, "Fully automatic three-dimensional visualization of intravascular optical coherence tomography images: methods and feasibility in vivo," Biomed. Opt. Express **3**(12), 3291–3303 (2012).
14. S. Tsantis, G. C. Kagadis, K. Katsanos, D. Karnabatidis, G. Bourantas, and G. C. Nikiforidis, "Automatic vessel lumen segmentation and stent strut detection in intravascular optical coherence tomography," Med. Phys. **39**(1), 503–513 (2011).
15. S. Geman and C. Graffigne, "Markov random field image models and their applications to computer vision," in *Proceedings of the International Congress of Mathematicians* (Berkeley, CA, 1986), Vol. 1, p. 2.
16. A. G. Roy, S. Conjeti, S. G. Carlier, P. K. Dutta, A. Kastrati, A. F. Laine, N. Navab, A. Katouzian, and D. Sheet, "Lumen segmentation in intravascular optical coherence tomography using backscattering tracked and Initialized Random Walks," IEEE J. Biomed. Health Inform. **20**(2), 606–614 (2016).
17. Z. Wang, D. Chamie, H. G. Bezerra, H. Yamamoto, J. Kanovsky, D. L. Wilson, M. A. Costa, and A. M. Rollins, "Volumetric quantification of fibrous caps using intravascular optical coherence tomography," Biomed. Opt. Express **3**(6), 1413–1426 (2012).
18. Z. Wang, H. Kyono, H. G. Bezerra, H. Wang, M. Gargesha, C. Alraies, C. Xu, J. M. Schmitt, D. L. Wilson, M. A. Costa, and A. M. Rollins, "Semiautomatic segmentation and quantification of calcified plaques in intracoronary optical coherence tomography images," J. Biomed. Opt. **15**(6), 061711 (2010).
19. C. Chiastra, E. Montin, M. Bologna, S. Migliori, C. Aurigemma, F. Burzotta, S. Celi, G. Dubini, F. Migliavacca, and L. Mainardi, "Reconstruction of stented coronary arteries from optical coherence tomography images: Feasibility, validation, and repeatability of a segmentation method," PLoS One **12**(6), e0177495 (2017).
20. M. L. Olender, L. S. Athanasiou, J. M. de la Torre Hernández, E. Ben-Assa, F. R. Nezami, and E. R. Edelman, "A mechanical approach for smooth surface fitting to delineate vessel walls in optical coherence tomography images," IEEE Trans. Med. Imaging **38**(6), 1384–1397 (2019).

Biomedical Optics EXPRESS

21. H. Zhao, B. He, Z. Ding, K. Tao, T. Lai, H. Kuang, R. Liu, X. Zhang, Y. Zheng, J. Zheng, and T. Liu, "Automatic Lumen Segmentation in Intravascular Optical Coherence Tomography Using Morphological Features," IEEE Access **7**, 88859–88869 (2019).
22. L. S. Athanasiou, F. Rikhtegar, M. Z. Galon, A. C. Lopes, P. A. Lemos, and E. R. Edelman, "Fully automated lumen segmentation of intracoronary optical coherence tomography images," in *Medical Imaging 2017: Image Processing* (International Society for Optics and Photonics, 2017), Vol. 10133, p. 101332I.
23. L. Athanasiou, F. R. Nezami, M. Z. Galon, A. C. Lopes, P. A. Lemos, J. M. de la Torre Hernandez, E. Ben-Assa, and E. R. Edelman, "Optimized computer-aided segmentation and three-dimensional reconstruction using intracoronary optical coherence tomography," IEEE J. Biomed. Health Inform. **22**(4), 1168–1176 (2018).
24. M. Han, K. Kim, S.-J. Jang, H. S. Cho, B. E. Bouma, W.-Y. Oh, and S. Ryu, "GPU-accelerated framework for intracoronary optical coherence tomography imaging at the push of a button," PLoS One **10**(4), e0124192 (2015).
25. M. C. Moraes, D. A. C. Cardenas, and S. S. Furuie, "Automatic lumen segmentation in IVOCT images using binary morphological reconstruction," BioMed Eng OnLine **12**(1), 78 (2013).
26. M. C. Moraes and S. S. Furuie, "Automatic coronary wall segmentation in intravascular ultrasound images using binary morphological reconstruction," Ultrasound Med. Biol. **37**(9), 1486–1499 (2011).
27. K. N. Chaudhury and S. D. Dabhade, "Fast and provably accurate bilateral filtering," IEEE Trans. on Image Process. **25**(6), 2519–2528 (2016).
28. M. M. G. de Macedo, C. K. Takimura, P. A. Lemos, M. A. Gutierrez, M. M. G. de Macedo, C. K. Takimura, P. A. Lemos, and M. A. Gutierrez, "A robust fully automatic lumen segmentation method for in vivo intracoronary optical coherence tomography," Res. Biomed. Eng. **32**(1), 35–43 (2016).
29. H. M. Kim, S. H. Lee, C. Lee, J. Ha, and Y. Yoon, "Automatic lumen contour detection in intravascular OCT images using Otsu binarization and intensity curve," in *2014 36th Annual International Conference of the IEEE Engineering in Medicine and Biology Society* (2014), pp. 178–181.
30. H. S. Nam, C.-S. Kim, J. J. Lee, J. W. Song, J. W. Kim, and H. Yoo, "Automated detection of vessel lumen and stent struts in intravascular optical coherence tomography to evaluate stent apposition and neointimal coverage," Med. Phys. **43**(4), 1662–1675 (2016).